Modeling the Partial Oxidation of Methane in a Short Contact Time Reactor

ARTICLE *in* AICHE JOURNAL · NOVEMBER 1998

Impact Factor: 2.75 · DOI: 10.1002/aic.690441114

2 AUTHORS:

Olaf Deutschmann
Karlsruhe Institute of Technology
200 PUBLICATIONS **4,001** CITATIONS
SEE PROFILE

L. D. Schmidt
University of Minnesota Twin Cities
221 PUBLICATIONS **8,786** CITATIONS
SEE PROFILE

Modeling the Partial Oxidation of Methane in a Short-Contact-Time Reactor

Olaf Deutschmann and Lanny D. Schmidt
Dept. of Chemical Engineering and Materials Science, University of Minnesota, Minneapolis, MN 55455

Partial oxidation of methane in monolithic catalysts at very short contact times offers a promising route to convert natural gas into syngas (H_2 and CO), which can then be converted to higher alkanes or methanol. Detailed modeling is needed to understand their complex interaction of transport and kinetics in these systems and for their industrial application. In this work, the partial oxidation of methane in noble-metal (Rh and Pt)-coated monoliths was studied numerically as an example of short-contact-time reactor modeling. A tube wall catalytic reactor was simulated as a model for a single pore of the monolithic catalyst using a 2-D flow field description coupled with detailed reaction mechanisms for surface and gas-phase chemistry. The catalytic surface coverages of adsorbed species are calculated vs. position. The reactor is characterized by competition between complete and partial oxidation of methane. At atmospheric pressure, CO_2 and H_2O are formed on the catalytic surface at the entrance of the catalytic reactor. At higher pressure, gas-phase chemistry becomes important, forming more complete oxidation products downstream and decreasing syngas selectivity by about 2% at 10 bar. Temperature (from 300 to ~ 1,200 K), velocity, and transport coefficients change very rapidly at the catalyst entrance. The dependence of conversion and selectivity on reactor conditions was examined.

Introduction

Reaction engineering and combustion processes are very often characterized by a complex interaction of transport and chemical kinetics. The chemistry may include gas-phase as well as surface reactions such as in catalytic combustion and conversion of natural gas. The partial oxidation of methane, the main component of natural gas, in short-contact-time reactors has recently been shown to offer a promising route to convert natural gas into syngas (H_2 and CO) which subsequently can be converted to higher alkanes or methanol (Hickman and Schmidt, 1993; Bodke and Schmidt, 1998). The catalytic reactors used for these processes, such as foam or extruded monoliths, wire gauzes, or sintered spheres, are coated with noble metals such as platinum and rhodium. In particular, rhodium used with the appropriate support has been shown to produce syngas selectivity of over 90% with methane conversion of over 90% (Bodke and Schmidt, 1998). This process can be run autothermally and almost adiabatically with a residence time of approximately 1 ms. The short contact time guarantees a very high throughput using a small amount of catalyst and low energy and capital costs. The industrial application needs to operate at higher pressure, but high-pressure experiments in conventional laboratories are expensive and dangerous because the very reactive mixture may explode. Detailed modeling and simulation will help to understand the complex interactions between reactive flow and catalytic surface and can also be used to explore reactor conditions which are beyond available experimental facilities.

This simulation of fluid flows, including detailed schemes for surface and gas-phase chemistry, has recently received considerable attention due to the availability of faster computers, the development of new numerical algorithms, and the establishment of elementary reaction mechanisms. A key problem still remaining is the stiffness of the governing equations because of different time scales introduced by chemical reactions including adsorption and desorption. Therefore, simulations often use a simplified model, either of the flow

Correspondence concerning this article should be addressed to L. D. Schmidt.
Current address of O. Deutschmann: Heidelberg University, IWR, D-69120 Heidelberg, Germany.

field or chemistry. This simplification can be risky if a strong interaction exists between flow and chemistry.

Previous studies have often assumed a plug-flow tubular reactor model (PFTR) where radial mass and heat transfer are either neglected or included only through effective mass- or heat-transfer coefficients. The resulting initial value problem is easy to solve, even for a system involving many equations. This method was applied by Hickman and Schmidt (1993) to establish surface reaction mechanisms for high-temperature methane oxidation on Pt and Rh. An extended PFTR simulation by Goralski (Schmidt et al., 1998) also included detailed gas-phase chemistry which allowed extension of the investigation to higher pressure.

Catalytic combustion of methane in stagnation flows was simulated by Deutschmann et al. (1996) and Raja et al. (1998) using transient 1-D models. The transition from heterogeneous to homogeneous oxidation of methane on a platinum foil (formation of a flame in front of the foil) was simulated using detailed gas and surface chemistry models in one of these computer programs (Deutschmann et al., 1998a). Veser et al. (1997) used a 1-D model coupled with a detailed surface-reaction mechanism to carry out a dynamic simulation of the ignition behavior of a monolithic reactor for syngas formation. A boundary layer model including detailed chemistry was successfully applied by Warnatz et al. (1994) to simulate catalytic oxidation over flat plates, although diffusion in flow direction was still neglected.

We use a 2-D elliptic model to simulate a short-contact-time reactor. The flow is laminar and the transport coefficients depend on composition and temperature. Elementary surface reaction mechanisms are used to calculate the surface mass fluxes. The coverage of the catalytic wall with adsorbed species is calculated as a function of the position in the reactor. In earlier 2-D numerical studies of short-contact-time reactors (Deutschmann and Schmidt, 1998b; Schmidt et al., 1998), we included only the surface chemistry. In the present work, a gas-phase reaction mechanism is also included in the model. Simulations are carried out using the commercial computational fluid dynamics (CFD) code FLUENT (FLUENT, 1997), which is coupled to newly developed external subroutines that model the chemistry.

In this study, the partial oxidation of methane in a tubular reactor with a noble metal catalytic surface (Pt or Rh) is studied numerically using a detailed description of the flow field and chemistry. The competition between complete and partial oxidation, the role of surface kinetics, and the complex behavior at the catalyst entrance region are discussed. The dependence of conversion and selectivity on catalyst material, flow velocity, pore diameter, methane/oxygen ratio, and pressure is calculated, and the influence of gas-phase chemistry on selectivity and conversion is considered.

Mathematical and Numerical Model

The numerical simulation is based on the CFD code FLUENT. The code is well established and can easily be used to set up and solve fluid flow problems. However, modeling of detailed chemistry in current versions is limited because of a maximum number of reactions and difficulties in handling stiff chemistry. Furthermore, FLUENT's surface reaction model does not account for the surface coverage. Therefore, we coupled the FLUENT code to external subroutines that model detailed gas-phase and surface chemistry.

Conservation equations

The basic conservation equations as used in FLUENT for laminar flow fields are summarized in this section. A mass source term, gravitational and external body forces, thermal diffusion, and viscous heating are not used in our simulations, resulting in the following equation system

continuity equation:
$$\frac{\partial \rho}{\partial t} + \frac{\partial}{\partial x_i}(\rho u_i) = 0 \quad (1)$$

momentum conservation equation:
$$\frac{\partial}{\partial t}(\rho u_i) + \frac{\partial}{\partial x_j}(\rho u_i u_j) = -\frac{\partial p}{\partial x_i} + \frac{\partial \tau_{ij}}{\partial x_j} \quad (2)$$

with the stress
$$\tau_{ij} = \left[\mu\left(\frac{\partial u_i}{\partial x_j} + \frac{\partial u_j}{\partial x_i}\right)\right] - \frac{2}{3}\mu\frac{\partial u_l}{\partial x_l}\delta_{ij} \quad (3)$$

species conservation equation:
$$\frac{\partial}{\partial t}(\rho Y_i) + \frac{\partial}{\partial x_j}(\rho u_j Y_i) = -\frac{\partial}{\partial x_j}(j_{i,j}) + R_i \quad (i = 1, \ldots, N_g) \quad (4)$$

with diffusion mass flux
$$j_{i,j} = -\rho D_{i,m}\frac{\partial Y_i}{\partial x_j} \quad (5)$$

enthalpy conservation equation:
$$\frac{\partial}{\partial t}(\rho h) + \frac{\partial}{\partial x_j}(\rho u_j h) = \frac{\partial}{\partial x_j}\left(k\frac{\partial T}{\partial x_j}\right) - \frac{\partial}{\partial x_j}\sum_i^{N_g} h_i j_{i,j} + \frac{\partial p}{\partial t} + u_j\frac{\partial p}{\partial x_j} + \sum_i^{N_g} h_i R_i \quad (6)$$

Here, ρ = density, t = time, x_i = Cartesian coordinates ($i = 1, 2, 3$), u_i = Cartesian components of the velocity vector, p = static pressure, Y_i = mass fraction of species i, R_i = net rate of production of species i due to chemical reactions, $D_{i,m}$ = diffusion coefficient of species i in the mixture, h = static enthalpy, T = temperature, h_i = enthalpy of species i, and N_g = number of gas-phase species. The Einstein convention is adopted in these equations, that is, whenever the same index appears twice in any term, summation over the range of that index is implied.

The density is computed via the ideal gas law. The viscosity, μ; the thermal conductivity, k; and the diffusion coefficient of species i in the mixture, $D_{i,m}$, depend on the local composition and on temperature, and they are calculated via kinetic theory.

The enthalpy is defined as

$$h = \sum_i^{N_g} Y_i h_i \quad \text{with} \quad h_i = \int_{T_{\text{ref}}}^{T} c_{p,i}\,dT \quad (7)$$

where T_{ref} is a reference temperature and $c_{p,i}$ is the specific

heat at constant pressure of species i. $c_{p,i}$ is modeled as a polynomial function of temperature.

FLUENT solves the conservation equations using a control volume–based finite difference method. A nonstaggered system is applied for storage of discrete velocities and pressure. The resulting equations are solved using SIMPLE-like algorithms with an iterative line-by-line matrix solver and multigrid acceleration.

Gas-phase chemistry model

Chemical reactions in the gas phase lead to source terms in the species and enthalpy conservation Eqs. 4 and 6. These source terms R_i are given as the mass rate of creation and depletion of species i by chemical reactions. They are calculated in user-defined external subroutines and are provided to the code at each fluid flow cell for every iteration.

The chemistry is modeled by elementary reactions on a molecular level. The chemical source terms R_i are given as

$$R_i = M_i \sum_{k=1}^{K_g} \nu_{ik} k_{f_k} \prod_{j=1}^{N_g} [X_j]^{\nu'_{jk}} \quad (i = 1, \ldots, N_g), \tag{8}$$

where M_i is the molar mass of species i, K_g is the number of elementary gas-phase reactions, ν_{ik} (right side minus left side of reaction equation) and ν'_{jk} (left side of reaction equation) are stoichiometric coefficients, k_{fk} is the forward rate coefficient, and $[X_j]$ the concentration of species j. The temperature dependence of the rate coefficients is described by a modified Arrhenius expression

$$k_{f_k} = A_k T^{\beta_k} \exp\left[\frac{-E_{a_k}}{RT}\right] \tag{9}$$

with A_k as preexponential factor, β_k as temperature coefficient, E_{a_k} as activation energy, and R as the gas constant.

Because the chemical reaction systems are stiff, a direct calculation of the chemical source terms R_i by Eq. 8, using the given temperature and concentrations, may easily lead to divergence or oscillations of the iterative solution procedure. Therefore, a pseudotime integration is introduced to calculate the chemical source term. The given local concentrations $[X_i]$ are used as initial values (t_0) of the nonlinear ordinary differential equation (ODE) system

$$\frac{\partial [X_i]}{\partial t} = \frac{R_i([X_i], T)}{M_i} = \sum_{k=1}^{K_g} \nu_{ik} A_k T^{\beta_k} \times \exp\left[\frac{-E_{a_k}}{RT}\right] \prod_{j=1}^{N_g} [X_j]^{\nu'_{jk}} \quad (i = 1, \ldots, N_g) \tag{10}$$

where the right-hand side represents Eq. 8. The ODE system (Eq. 10) is integrated over a small time period Δt to give the local chemical source term of species i:

$$R'_i = M_i \frac{[X_i](t_0 + \Delta t) - [X_i](t_0)}{\Delta t} \tag{11}$$

This source term R'_i is then returned to the FLUENT code. The temperature is kept constant during the integration of system Eq. 8. The value of Δt is chosen to be much smaller than the local time scales of diffusion and convection. This procedure accounts for the variation of the species concentrations due to chemical reactions on a small time scale. The ODE system Eq. 8 is solved by an implicit extrapolation solver that is based on the software package LIMEX (Deuflhard et al., 1987). In this solver, the Jacobian of the system Eq. 8 has to be calculated. We provide an analytical Jacobian to speed up the simulation. The form of the Jacobian is automatically generated from the reaction mechanism during initialization of the detailed chemistry module, so a change in the kinetics does not cause any additional effort. The use of the pseudotime integration drastically improves the numerical stability when the residuals of the species variables are large, mainly in the beginning of the iterative solution procedure.

Because the chemical source terms have to be calculated for each fluid cell and for each iteration step, the total CPU time needed to achieve convergence increases dramatically if detailed gas-phase chemistry is used.

Surface chemistry model

Chemical reactions on the catalytic reactor wall lead to the following boundary conditions

$$\dot{s}_i M_i = \left(\vec{j}_i + \rho Y_i \vec{u}\right)\vec{n} \quad (i = 1, \ldots, N_g) \tag{12}$$

where $\dot{s}_i$ is the creation or depletion rate of species i by adsorption and desorption processes, $\vec{j}_i$ the diffusive flux and Y_i the mass fraction of species i in the gas phase adjacent to the surface, $\vec{u}$ the Stefan velocity, and $\vec{n}$ the unit vector normal to the surface.

The state of the catalytic surface is described by its temperature and the coverages of adsorbed species that vary in the flow direction. We have developed subroutines to calculate the surface coverages (Θ_i, the fraction of surface sites covered by species i) and the surface mass fluxes ($\dot{s}_i M_i$) at the catalytic wall. At each catalytic wall cell, the surface mass fluxes are provided for the FLUENT code. The surface chemistry is also modeled by elementary reactions similar to the gas-phase reaction model. The chemistry source terms, $\dot{s}_i$, of gas-phase species due to adsorption/desorption and surface species (adsorbed species) are given by

$$\dot{s}_i = \sum_{k=1}^{K_s} \nu_{ik} k_{f_k} \prod_{j=1}^{N_g + N_s} [X_j]^{\nu'_{jk}} \quad (i = 1, \ldots, N_g + N_s) \tag{13}$$

where K_s is the number of elementary surface reactions (including adsorption and desorption), ν_{ik} and ν'_{jk} are the appropriate stoichiometric coefficients (see above), and N_s is the number of species adsorbed. The concentration $[X_i]$ of an adsorbed species is given in mol/m^2 and equals the surface coverage (Θ_i) multiplied by the surface site density (Γ).

The temperature dependence of the rate coefficients is described by a modified Arrhenius expression

$$k_{f_k} = A_k T^{\beta_k} \exp\left[\frac{-E_{a_k}}{RT}\right] \prod_{i=1}^{N_s} \Theta_i^{\mu_{ik}} \exp\left[\frac{\epsilon_{i_k} \Theta_i}{RT}\right] \tag{14}$$

This expression takes an additional coverage dependence into account using the parameters μ_{ik} and ϵ_{ik}. The factor Θ^{μ} has to be considered in relation to the factor $[X]^{\nu}$ in Eq. 13.

In our calculations we are interested in the steady-state solution. Hence, the time variation of the surface coverage (Θ_i) is zero

$$\frac{\partial \Theta_i}{\partial t} = \frac{\dot{s}_i}{\Gamma} = 0 \quad (i = N_g + 1, \ldots, N_g + N_s) \tag{15}$$

In external subroutines, this equation system is solved to obtain surface coverages and surface mass fluxes. Here, FLUENT provides the concentration of the gas-phase species and the temperature at each computational cell with a catalytic wall as boundary. In the surface chemistry module, coverages and surface mass fluxes are calculated for each "global" iteration, keeping the local species concentrations and temperature constant. The algebraic equation system (Eq. 15) is either solved by Newton's method or by a time integration of the corresponding ODE system until a steady state is reached. An implicit method based on LIMEX (Deuflhard et al., 1987) is used for the time integration. We provide an analytical Jacobian that is automatically generated from the surface reaction mechanism. The coverage data of the former iteration are used as initial conditions for the next step, and, if possible, the system (Eq. 15) is not solved for each iteration step using former calculated surface mass fluxes. Both of these features result in a reduction of CPU time. However, an additional underrelaxation of the variation of the surface mass fluxes may be necessary, such as when a species that is largely produced on the surface has a high sticking coefficient such as CO in our examples.

Geometry and boundary conditions

The laboratory-scale short-contact-time reactor and tubular reactor model studied in the present work are shown in Figure 1. This tubular reactor serves as a model for a single pore of the monolithic catalyst. Typical pore diameter varies between 0.25 and 1 mm (80 to 20 pores per linear inch), while the length of the catalytic part of the reactor is typically 1 cm. In these small-diameter channels, the flow field is always laminar with a Reynolds number of approximately 20, which has the same order of magnitude at the inlet and under reactor conditions. Experimental measurements indicate only small temperature gradients over the catalyst for situations studied in this work. Hence, the catalytic wall can be assumed to be isothermal. An adiabatic, chemically inert wall, 1 cm in length, is used in the model to simulate the experimentally used heat shields in front of and behind the catalytic section.

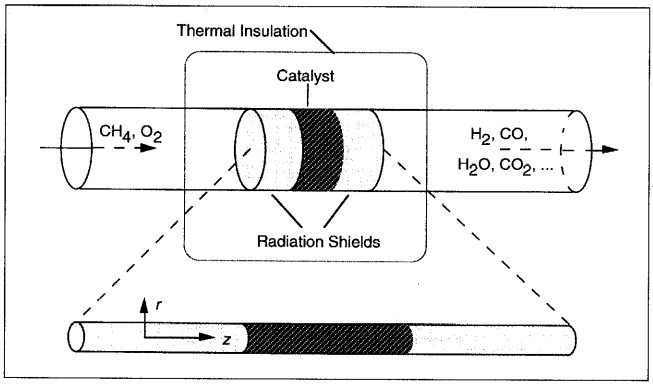

Figure 1. Laboratory-scale short-contact-time reactor (top) and tubular reactor model representing a single pore of the monolith (bottom).

The tube wall catalytic reactor is described by the 2-D conservation equations using cylindrical geometry. Hence, the conservation Eqs. 1–6 are transformed into cylindrical coordinates where the axial direction, z, and the radial direction, r, are the independent variables. In the radial direction, the equations are solved between $r = 0$ and $r = d/2$ with d as tube (channel) diameter.

The flow enters the computational domain ($z = -1$ cm, r) at a known velocity, composition, and temperature. A flat profile of the axial velocity, u, and a vanishing radial velocity, $v = 0$, is used in all simulations at this inlet boundary. At the tube wall (z, $r = d/2$), axial and radial velocities are constrained to zero. At the tube centerline (z, $r = 0$), a symmetry boundary condition is applied at which all variables have a zero normal gradient, except the velocity component normal to the boundary. This normal velocity vanishes at the symmetry boundary. At the reactor exit ($z = 2$ cm, r), an outlet boundary is applied at which values for all variables are extrapolated from the interior cells adjacent to the outlet.

A structured grid is used for the simulation; the grid must be very fine around the catalyst entrance to resolve the flow field. The total number of grid points varied between 10^3 and 10^4 depending on reactor diameter and external conditions such as temperature. The number of computational cells with surface reaction boundaries varied between 30 and 100. The numerical calculations were performed on a Cray C916/12512. Typically, a CPU time of about 20 min was required to obtain a converged solution for a simulation where gas-phase chemistry could be excluded (but with surface chemistry). If detailed gas-phase chemistry is additionally taken into account, the CPU time easily exceeded 10 h.

Chemical Reaction System

The formation of syngas (H_2 and CO) from methane/oxygen (or methane/air) mixtures on noble metal catalysts is characterized by the competition between a complete oxidation channel globally written as

$$CH_4 + 2O_2 \rightarrow CO_2 + 2H_2O \quad \Delta H_R = -890 \text{ kJ/mol}$$

and a partial oxidation channel written as

$$CH_4 + 1/2O_2 \rightarrow CO + 2H_2 \quad \Delta H_R = -36 \text{ kJ/mol}$$

Appropriate catalytic material and residence time must be chosen to achieve high syngas selectivity. Rhodium-coated foam catalysts with a residence time of approximately 1 ms are capable of producing this high syngas selectivity (>90%) with a high methane conversion (>99%) (Bodke and Schmidt, 1998).

The oxidation of methane can occur both on the surface and in the gas phase. It is generally assumed that the influence of gas-phase chemistry on the overall conversion can be neglected at atmospheric pressure because the residence time is on the order of a few milliseconds, a time that is too short to ignite the mixture homogeneously. Furthermore, the radicals formed in the gas phase may recombine on the surface of the small diameter channel, inhibiting a chain-branching reaction. However, we expect the role of gas-phase chemistry to increase with increasing pressure.

Gas-phase reaction mechanism

The gas-phase reaction scheme is based on an elementary step mechanism developed for hydrocarbon oxidation by Warnatz et al. (1998). The original mechanism is reduced by calculation of a homogeneous reactor under the given conditions in order to keep the 2-D simulation tractable. This reduction results in a mechanism of 164 reactions among 22 chemical species which were finally used for the simulation. The crucial steps of the gas-phase conversion of methane under given conditions are as follows. Hydrogen abstraction from the methane molecule occurs mainly by H, O, and OH radicals, which leads to CH_3 radicals. These radicals will either be oxidized to CO and CO_2 via intermediates such as CH_3OH, CH_2OH, CH_3O, CH_2O, CH, CH_2, and CHO, or they can recombine to C_2H_6. Ethane can subsequently be dehydrogenated to ethylene.

A radical pool must be established before gas-phase conversion is fast enough to compete with catalytic conversion. Furthermore, the presence of oxygen is a prerequisite for significant methane conversion in the gas phase: if the catalytic conversion is very fast, all the oxygen is already consumed before significant gas-phase conversion can take place. Therefore, the detailed description of mass transport that may be rate-limiting for the catalytic conversion is also important to elucidate the role of gas-phase chemistry. Because of the fast complete oxidation channels, gas phase reactions are expected to decrease syngas selectivity. Aside from this decrease in reactor performance, gas-phase chemistry has the potential of flames and explosions and must be understood from a reactor safety point of view.

Surface-reaction mechanism

Hickman and Schmidt (1993) developed a detailed surface reaction mechanism for high-temperature partial oxidation of methane in a short-contact-time reactor with a Rh- or Pt-coated foam monolith. These mechanisms are used without modification in the present study. Table 1 summarizes the reaction steps with their associated rate expressions. The reaction scheme assumes dissociative methane and oxygen adsorption; formation of CO, CO_2, H_2, and H_2O via OH; and desorption of products. All reaction steps are reversible except methane adsorption and CO_2 desorption. It is assumed that oxygen is adsorbed noncompetitively with other species whereas all other species are adsorbed competitively. The site density (Γ) is assumed to be 1.67×10^{-5} mol/m^2, which is 10^{15} atoms/cm^2. More details such as reaction order can be found in the original work (Hickman and Schmidt, 1993).

The reaction mechanisms were developed using a plug-flow tubular reactor model, where mass- and heat-transport effects cannot easily be taken into account. However, the model predicts selectivity and conversion close to those observed over monolithic catalysts in an atmospheric-pressure, laboratory-scale reactor, and the differences between the catalysts (Pt and Rh) could be explained by comparison of individual reaction steps. The kinetic data of these mechanisms were taken either from the literature or from fits to experiments. Recent studies have shown that some features of the mechanisms need to be improved to be valid for a wider range of applications. Furthermore, adsorption of radicals such as H,

Table 1. Surface-Reaction Mechanism of Partial Oxidation of Methane on Rhodium and Platinum

Reaction				Rhodium			Platinum		
				A	E_a	s	A	E_a	s
CH_4*		→ C	+4H	1.9×10^{19}	21.0		3.3×10^{19}	43.1	
O_2*		→ 2O				0.01			0.003
H_2*		→ 2H				0.16			0.05
CO*		→ CO				0.50			0.84
H_2O*		→ H_2O				0.16			0.10
2O		→ O_2*		3.0×10^{21}	293.3		3.0×10^{21}	218.0	
2H		→ H_2*		3.0×10^{21}	75.4		3.0×10^{21}	75.4	
CO		→ CO*		4.0×10^{13}	$132.4-44.4\Theta_{CO}$		1.0×10^{13}	125.7	
H_2O		→ H_2O*		1.0×10^{13}	45.2		1.0×10^{13}	45.2	
H	+O	→ OH		4.2×10^{21}	83.8		6.0×10^{23}	10.5	
OH		→ O	+H	6.0×10^{21}	21.0		6.0×10^{16}	21.0	
H	+OH	→ H_2O		1.8×10^{26}	33.5		5.4×10^{25}	62.8	
H_2O		→ H	+OH	3.0×10^{23}	155.0		1.1×10^{22}	155.0	
OH	+OH	→ H_2O	+O	2.4×10^{24}	62.8		6.0×10^{23}	51.5	
C	+O	→ CO		3.0×10^{22}	62.8		3.0×10^{22}	62.8	
CO		→ C	+O	6.0×10^{19}	167.6		6.0×10^{19}	184.3	
CO	+O	→ CO_2*		6.0×10^{20}	104.7		6.0×10^{23}	100.5	
OH		→ OH*		8.1×10^{11}	142.5		1.5×10^{13}	201.1**	

Units: A [cm, mol, s], E_a [kJ/mol], s [—]; taken from Hickman and Schmidt (1993).
*Gas-phase species.
**Not used in all calculations.

O, and OH should be taken into account. Recombination of radicals on the catalytic surface will influence the role of gas-phase chemistry at higher pressure. Improved mechanisms are under development.

Results and Discussion

In this section, the syngas formation on Rh at atmospheric pressure is first discussed as a baseline case. Then the behavior at the catalyst entrance region is considered, and the results of the parameter studies, such as the dependence of selectivity and conversion on temperature, pressure, catalytic material, pore diameter, and the methane/oxygen ratio are discussed.

Rh catalyst at atmospheric pressure

The simulation of the following case will be discussed as a first example of catalytic methane oxidation in short-contact-time reactors: a methane/oxygen mixture (volumetric ratio 1.8, 30% nitrogen dilution) flows at a uniform inlet velocity of 1 m/s and at 298 K and at total pressure of 1.4 bar into a cylindrical tube 3 cm in length with a diameter of 0.5 mm as sketched in Figure 1. The 1-cm-long catalytic wall has no temperature gradient in the axial direction. The catalyst is rhodium, which is assumed to be a film on the wall. The wall is assumed to be adiabatic and chemically inert before and after the catalytic section.

The conditions are close to those in experiments carried out by Bodke and Schmidt (1998), in which a 65 ppi Rh/α-Al_2O_3 foam monolith was used as catalyst, although we simulate the foam as a straight channel 0.5 mm in diameter rather than the averaged 0.31-mm-diameter cell size of the foam. An autothermal reactor temperature of 1073 K was measured by a Pt/Pt-13%Rh thermocouple with an accuracy of ± 50 K and no axial temperature gradients were reported. In the experiment, oxygen was completely consumed inside the reactor. The methane conversion was 88.9%, the C atom selectivity to CO was 93.5% (6.5% to CO_2) and the H atom selectivity to H_2 was 91.0% (9% to H_2O). These data result in a calculated adiabatic reactor temperature of 1,090 K, which agrees with the measured temperature.

This simulation includes both surface and gas-phase chemistry. Figure 2 shows the calculated mass fractions of the reactants CH_4 and O_2 and the products CO, H_2, CO_2, and H_2O as a function of position in the reactor. The catalytic part of the tubular reactor is between 0 and 10 mm axial position (z) and the radial position (r) is set to zero at the tube axis so that the catalytic wall is at $r = 0.25$ mm. The flow direction is from left to right. Methane oxidation starts directly at the catalyst entrance where large radial and axial gradients are formed. At the catalyst exit, however, there is still some methane left, the methane conversion being 90.1%. In contrast to methane, oxygen is completely (99.96%) consumed in the catalytic reactor.

The formation of hydrogen and carbon monoxide as the desired products and water and carbon dioxide as the undesired products starts at the catalyst entrance. The strong radial profiles indicate that methane is almost completely oxidized by surface reactions as discussed in more detail below. Inside the first section of the catalyst, a competition between partial and complete oxidation paths occurs. In the beginning the oxygen concentration is large enough to quickly produce a significant amount of CO_2 and H_2O leading to steep radial concentration gradients of these species. The desorbed water can again be readsorbed. In contrast to H_2O, the adsorption of CO_2 molecules is negligible due to the very low heat of adsorption for CO_2 on Rh. These kinetic differences and the larger diffusion coefficient for water are responsible for the higher peak of CO_2 at the catalytic wall. Steam reforming, that is, the readsorption of the formed water, is not significant, as shown in Figure 2 where the H_2O mass fraction keeps constant behind the initial formation region, even though methane is still present. Because there is no CO_2 adsorption step in the surface reaction mechanism, CO_2 reforming cannot occur. One millimeter downstream from the catalyst entrance, the complete oxidation channels are practically extinguished, although considerable oxygen is still present in the gas phase. In this region oxygen is completely used for CO formation. The formation of syngas exceeds the formation of the combustion products even in the first part of the catalytic monolith. The higher diffusion coefficient of hydrogen compared to that of carbon monoxide leads to smaller radial gradients of H_2.

The role of gas-phase chemistry in the overall conversion at atmospheric pressure can be seen by the mass fractions of the minor species OH, CH_3, and C_2H_6, shown in Figure 3. The mass fraction of OH, which is one of the important radicals to initiate gas phase conversion, is very low, on the order of 10^{-10}. Furthermore, the OH peak occurs at a position in the reactor where methane and oxygen are already mostly consumed. Additionally, simulations with only surface chemistry and simulations with both surface and gas phase chemistry show no significant differences in total conversion and selectivity or in species concentration profiles. Hence, gas-phase chemistry does not play any role for syngas formation on Rh in short-contact-time reactors at atmospheric pressure.

Figure 3 illustrates the gas-phase reaction channels, although the mass fractions of OH, CH_3, and C_2H_6 are very low. The maximum OH occurs first because these radicals lead to H abstraction of the methane molecule, and consequently the CH_3 peak occurs downstream. Farther downstream, C_2H_6, made from CH_3 recombination, reaches its maximum. The C_2H_6 disappears again because there is still enough oxygen left to burn ethane.

The calculation of surface coverage as a function of the axial position in the reactor is shown in Figure 4. In the catalyst entrance region, the major surface species are CO(s), H(s), and O(s). In this region, the oxygen concentration is still large, explaining the CO_2 and H_2O formation. CO(s) is formed very fast from C(s) after dissociative methane adsorption. The rate-limiting step for water production is the OH(s) formation because OH(s) immediately leads to water because of the high hydrogen coverage, H(s). This fast OH(s) consumption also results in OH(s) coverage being lower than 10^{-7}. The activation energy for CO_2 formation is similar to that of OH formation, which results in the production of CO_2. Farther downstream, the oxygen coverage rapidly decreases, and therefore, any adsorbed oxygen is consumed by CO(s) formation which desorbs before it can be completely oxidized.

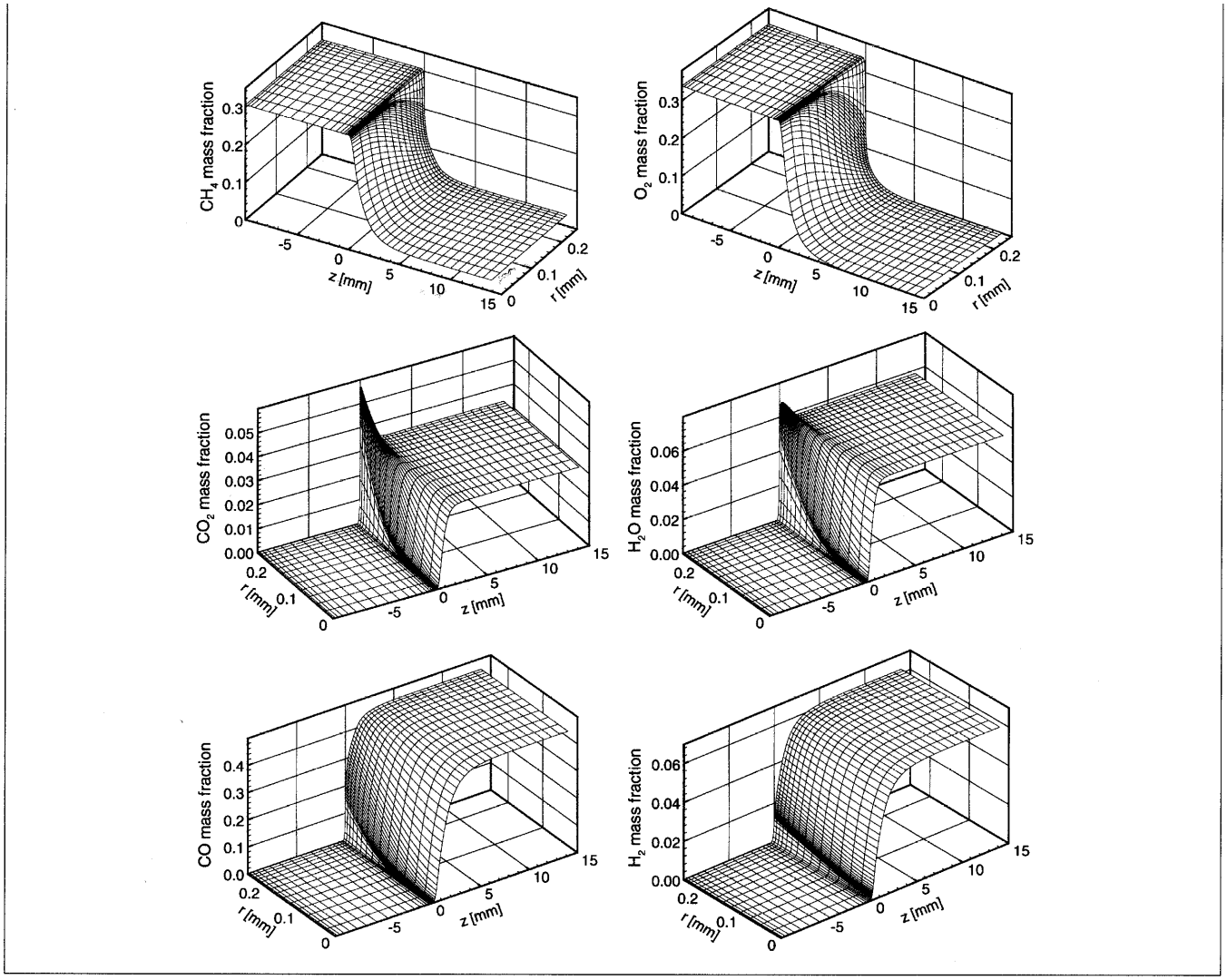

Figure 2. Mass fraction of CH_4, O_2, CO_2, H_2O, CO, and H_2 as a function of position in the reactor.

The axial position (z) is zero at the catalyst entrance and the catalytic wall is at the radial position (r) of 0.25 mm. The simulation includes gas-phase chemistry.

The straight channel geometry is obviously a simplification of a foam monolith where the pores vary in diameter and length and may be connected. Furthermore, the surface reaction mechanism was established by fitting the experimental results to a 1-D model that neglects transport effects (Hickman and Schmidt, 1993). However, the calculated selectivities (C and H atom based, respectively) and conversion agree quite well with the experimental data: CH_4 conversion is 90.1% (experiment: 88.9%), O_2 conversion is 99.96% (100%), H_2 selectivity is 90.6% (91.0%), and CO selectivity is 95.5% (93.5%). The calculated temperature of the catalytic part of the reactor wall is 1070 K, which is determined from conversion and selectivity assuming a "global" adiabatic process.

The thermodynamic equilibrium composition at 1070 K would lead to a complete (99.99%) methane conversion and H_2 and CO selectivities of 96.7% and 95.3%, respectively. Hence, the equilibrium CH_4 conversion is not reached yet at the reactor exit. Steam reforming could lead to an increase in CH_4 conversion and H_2 selectivity that is closer to thermodynamic equilibrium. However, steam reforming is too slow in the conditions discussed above to cause this increase.

Behavior at the catalyst entrance

When the cold inlet mixture enters the hot catalytic part of the reactor, an extremely fast variation of temperature, velocity, and transport coefficients of the reacting mixture occurs. This variation cause a strong disturbance of the parabolic flow field and two-dimensional effects in heat and mass transfer. Furthermore, a significant amount of the chemistry takes place in the entrance region of the catalyst.

In Figure 5 the temperature, axial velocity, viscosity, and thermal conductivity around the catalyst entrance are shown. The temperature increases to 1,000 K within about 1 mm, which corresponds to only two tube diameters. Simulations using different tube diameters show an even smaller entrance

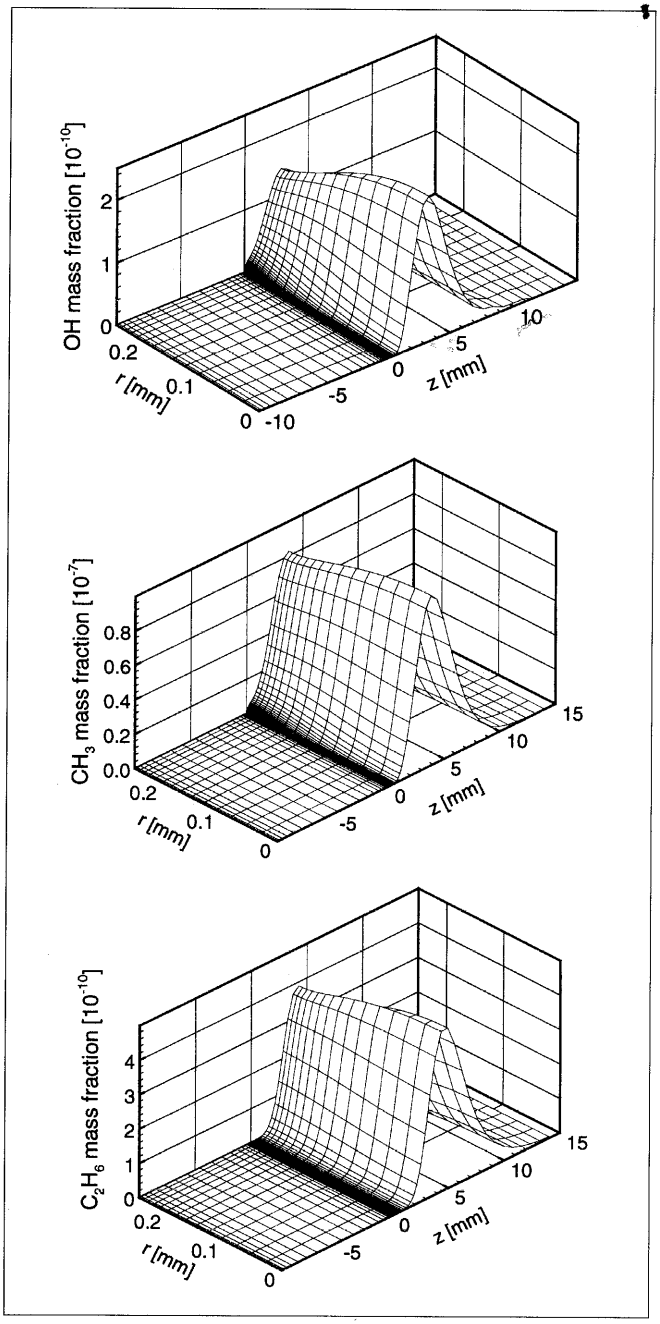

Figure 3. Mass fraction of OH, CH_3, and C_2H_6 as a function of position in the reactor.

The axial position (z) is zero at the catalyst entrance and the catalytic wall is at the radial position (r) of 0.25 mm. The simulation includes gas-phase chemistry.

region of one tube diameter length for a 0.25-mm-diameter pore. The pores of the frequently used 80 ppi (pores per inch; 3 pores/mm) monolith have approximately this small diameter.

The incoming gas is preheated immediately in front of the catalyst by upstream thermal conductivity in the gas. We note that radiation is not explicitly taken into account because the large thermal conductivity of the monolith results in an

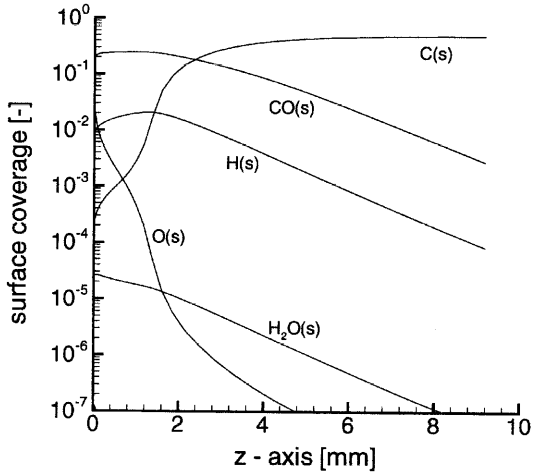

Figure 4. Surface coverage as a function of the axial position (z) in the reactor.

The axial position is zero at the catalyst entrance. The simulation includes gas-phase chemistry.

isothermal wall, and in the experiment, heat shields are used in front of and behind the hot catalytic reactor section.

The rapid increase of the velocity from 1 m/s to greater than 10 m/s at the catalyst entrance is not only a result of the density change due to the temperature increase but also of the change of the composition that leads to almost two moles

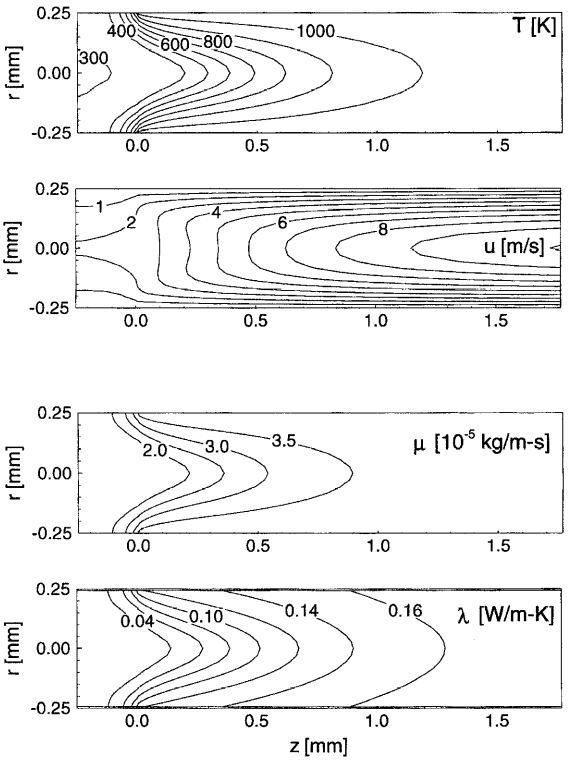

Figure 5. Temperature (T), axial velocity (u), viscosity (μ), and thermal conductivity (λ) around the catalyst entrance ($z = 0$).

The simulation includes gas-phase chemistry.

of products for each reactant under given conditions. In the first noncatalytic section of the tubular reactor a parabolic flow field is quickly established. At the catalyst entrance, this parabolic flow field is strongly perturbed and two maxima occur. This is shown by the 4 m/s contour line in Figure 5. A few tube diameters downstream, the parabolic velocity field is again established.

The rapid variation of the transport coefficients at the catalyst entrance is caused by the temperature increase and the composition change. In the simulation, we use detailed transport models in which the transport coefficients are a function of composition and temperature. Figure 5 also shows the variation of viscosity and thermal conductivity at the catalyst entrance. The rise of the thermal conductivity once again leads to an acceleration of the gas temperature increase. The diffusion coefficients vary approximately by a factor of 10 at the catalyst entrance. The variation of the transport coefficients due to chemical reaction is mainly caused by hydrogen formation because the hydrogen mole fraction increases to ~ 0.5 during the reaction.

As discussed above, the entire formation of undesired products at atmospheric pressure as well as the majority of syngas production takes place in the first part of the catalyst. Therefore, a detailed description is essential to model short-contact-time reactors and to understand the overall process.

Pt vs. Rh

Rhodium has been shown to be a better catalytic material for partial oxidation of methane (syngas formation) than platinum (Hickman and Schmidt, 1993). In contrast, platinum is favored as a catalyst for complete oxidation (catalytic combustion) of methane (Deutschmann et al., 1996) and can be used in catalytic burners and catalytic gas turbines. The different behavior can be explained by the processes on the catalytic surface.

The numerical code was used to simulate the reactor with either Rh- or Pt-coated monoliths under similar external conditions: inlet velocity of 1 m/s, methane/oxygen ratio of 1.8, inlet temperature of 298 K at 1.4 bar. These conditions are chosen to represent the experimental data (Hickman and Schmidt, 1993). Because it was shown above that gas-phase chemistry is negligible at atmospheric pressure, from now on all simulations (except for high pressures) are carried out with only a surface chemistry model, neglected all gas-phase reactions.

The simulation reproduces the experimental trends between Rh and Pt. Oxygen is completely consumed on both catalysts, but the selectivities vary: H_2 selectivity is 94% on Rh and only 56% on Pt, CO selectivity is 98% on Rh and 93% on Pt. Hence, the conversion of methane on Rh is much higher than on Pt (97% vs. 57%). The surface coverages on Pt and Rh are shown in Figure 6. Oxygen, only available in the entrance region of the catalyst, reveals a much lower coverage on Pt than on Rh. On Pt, the activation energy of OH formation is much lower than for CO formation, so oxygen mainly forms water with hydrogen atoms that come from the decomposition of adsorbed methane molecules. The water molecules desorb very fast, leading to the high water selectivity of 44% on Pt (6% on Rh). The slightly smaller CO selectivity on Pt is caused by its faster CO_2 formation step. Because more oxygen is used for complete oxidation on Pt, the methane conversion is lower, and the surface is mainly covered by carbon atoms, also in the first part of the catalyst.

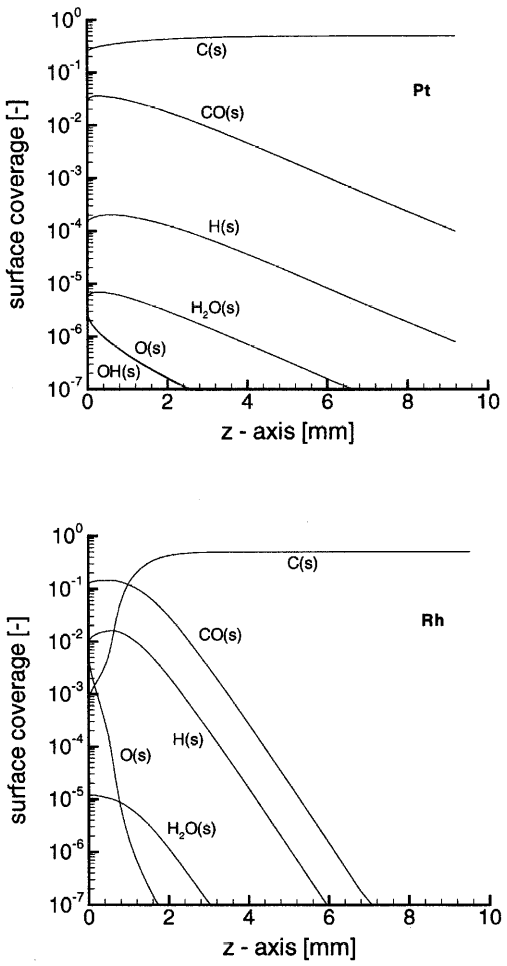

Figure 6. Surface coverage as a function of the axial position (z) for a platinum (top) and a rhodium (bottom) catalyst.

The axial position is zero at the catalyst entrance. The simulation does not include gas-phase chemistry.

Inlet velocity

The effect of inlet velocity on conversion and selectivity is studied for a methane/air mixture with CH_4/O_2 ratio of 1.8 at 1.4 bar and at a constant catalyst temperature of 1,280 K. The reactor diameter is 0.4 mm, the inlet temperature is 298 K, and platinum is chosen as catalyst. These conditions correspond to an experimental study with a 45 ppi Pt/Al_2O_3 foam monolith carried out by Hickman and Schmidt (1993).

The conversion of methane is predicted to decrease with increasing inlet velocity as shown in Figure 7. The selectivity of both hydrogen and carbon monoxide decreases slightly with increasing velocity. Figure 8 shows the temperature and gas-phase profile of oxygen for inlet velocities of 1 m/s and 10 m/s. For the faster flow, oxygen breakthrough occurs, so the reactor becomes too short for complete conversion. Because

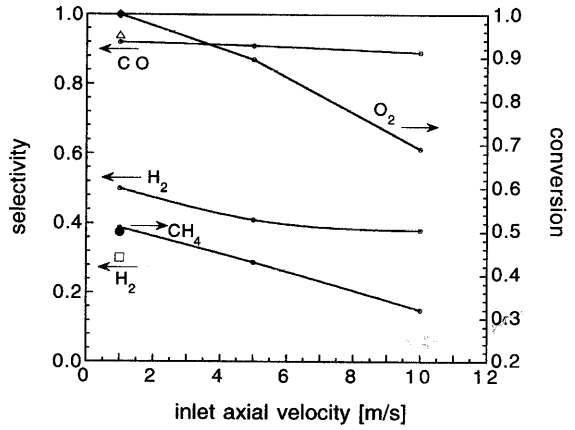

Figure 7. Syngas selectivity, methane and oxygen conversion as a function of inlet axial velocity.

Lines, simulations; symbols, experiment with a 45 ppi Pt/Al_2O_3 foam monolith (Hickman and Schmidt, 1993). The simulation does not include gas-phase chemistry.

the complete oxidation products H_2O and CO_2 are formed in the first part of the reaction, their selectivities increase with increasing velocity.

The gases do not reach the catalyst temperature in the 1-cm catalytic reactor section for higher flow velocities as shown in Figure 8. Here, axial catalyst temperature gradients can occur (Witt and Schmidt, 1996). A conductive wall boundary condition must be taken into account for a more accurate study of very fast flow rates. The solution of an energy balance inside the catalytic wall is beyond the scope of the present work but will be addressed in future investigations.

Pore diameter

The dependence of conversion and selectivity on pore diameter is shown in Figure 9. A rhodium catalyst at a constant temperature of 1,273 K (1,000°C) at 1.4 bar is simulated, the methane/oxygen ratio is 1.8 with 30% nitrogen as diluent, the inlet velocity is 1 m/s. Breakthrough of oxygen and methane occurs for pore diameter larger than 0.5 mm (40-ppi monolith). The CO selectivity remains almost constant while the hydrogen selectivity even increases slightly. The reason for that may be the larger radial concentration gradients for increasing tube diameter and the high hydrogen diffusion coefficient. Both effects can lead to a fast transport of hydrogen away from the catalytic wall, resulting in a shift of the hydrogen adsorption–desorption equilibrium towards desorption, thus increasing total hydrogen formation. The role of the tube diameter was investigated in a former study (Schmidt et al., 1998) in more detail.

Temperature

Short-contact-time reactors allow the running of the syngas formation on rhodium and platinum nearly autothermally and adiabatically if the reactor is insulated. Only small temperature gradients vs. the axial reactor position have been measured. The reactor temperature is determined by conversion, selectivity, and heat loss. A higher reactor temperature could

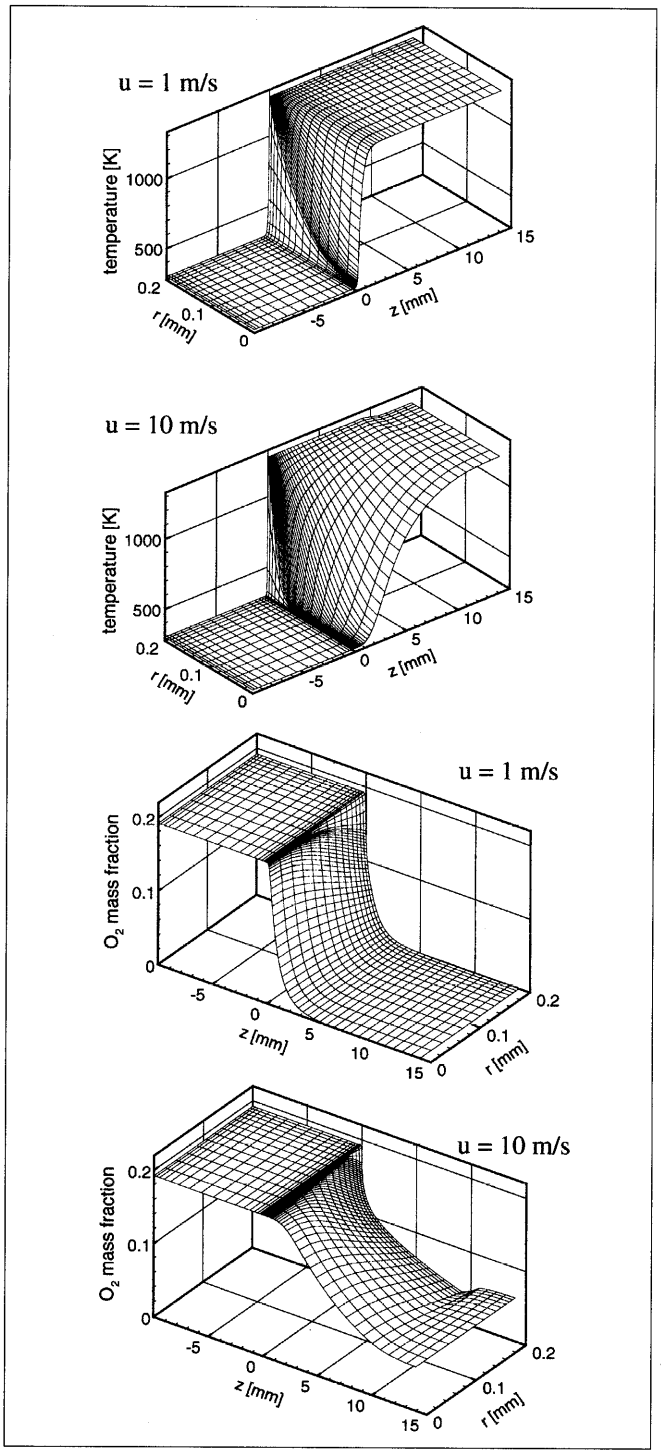

Figure 8. Temperature and oxygen profile for axial inlet velocities of 1 m/s and 10 m/s.

Pt catalyst, $d = 0.4$ mm, CH_4/O_2 ratio of 1.8 (methane/air mixture), $p = 1.4$ bar, $T_{cat} = 1280$ K. The axial position (z) is zero at the catalyst entrance, the catalytic wall is at the radial position (r) of 0.2 mm. The simulation does not include gas-phase chemistry.

be achieved by preheating the reactants. The influence of temperature variation on selectivity and conversion were numerically studied by varying the isothermal catalytic wall tem-

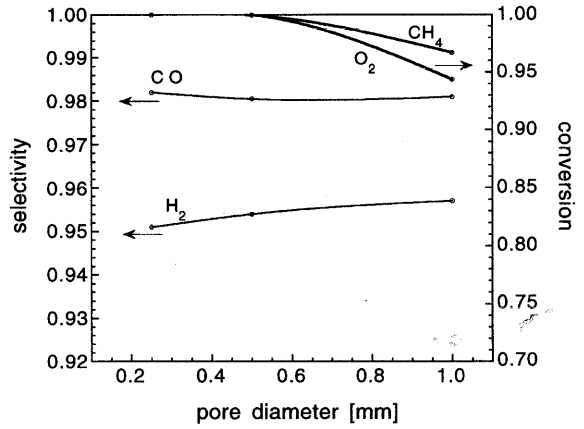

Figure 9. Syngas selectivity, methane and oxygen conversion as a function of pore diameter.

Rh catalyst, CH_4/O_2 ratio of 1.8 (30% N_2 as diluent), $p = 1.4$ bar, $T_{cat} = 1273$ K, $u_{in} = 1$ m/s. The simulation does not include gas-phase chemistry.

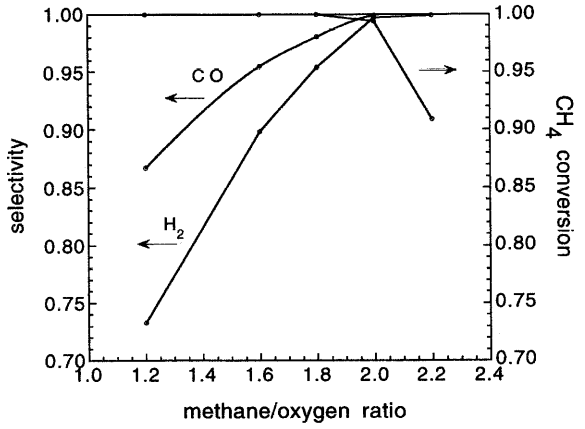

Figure 10. Syngas selectivity and methane conversion as a function of methane/oxygen ratio.

Rh catalyst, $d = 0.25$ mm, 30% N_2 as diluent, $p = 1.4$ bar, $T_{cat} = 1273$ K, $u_{in} = 1$ m/s. The simulation does not include gas-phase chemistry.

perature in a former investigation (Deutschmann and Schmidt, 1998). Conversion and syngas selectivity were found to increase with rising temperature. This tendency agrees with the experimental observation for preheated gases (Hickman and Schmidt, 1993). Using the conditions of the baseline case, the predicted conversion of methane increases from 84% at 1,023 K to 99% at 1,223 K. The CO and H_2 selectivities increase from 94% and 87% to 98% and 95%, respectively, over the same temperature range.

CH_4/O_2 ratio

The influence of the variation of methane/oxygen ratio is studied using the same conditions as for the pore diameter study, except the pore diameter is kept constant at 0.25 mm. A methane/oxygen ratio of about 1.8 was experimentally found to give the highest syngas yield in an authothermal and adiabatic reactor. In the simulation, where a constant temperature of 1,273 K is used, the maximum syngas yield was achieved at the stoichiometric (referring to syngas formation) methane/oxygen ratio of 2, as shown in Figure 10. The syngas selectivity decreases for leaner mixtures but methane is completely consumed. The syngas selectivity is almost 100% for more rich mixtures but the CH_4 conversion decreases. The chemical heat release, which is needed to run the process autothermally, mainly comes from CO_2 and H_2O formation. Therefore, for CH_4/O_2 ratios greater than ~ 2, the reactor temperature would drop unless the incoming mixture is preheated. A temperature decrease leads to lower syngas selectivity as discussed above.

Figure 11 shows that the surface coverages strongly vary for different CH_4/O_2 ratios. While C(s) is the primary surface species for richer mixtures, such as CH_4/O_2 ratio of 2.0, the surface is mainly covered by CO(s) for leaner mixtures, such as CH_4/O_2 ratio of 1.2. In the latter case, enough oxygen is available for consumption of adsorbed carbon, C(s). For even leaner mixtures, such as at conditions used for catalytic combustion of methane (CH_4/O_2 ratio smaller than 0.5), the major surface species is oxygen.

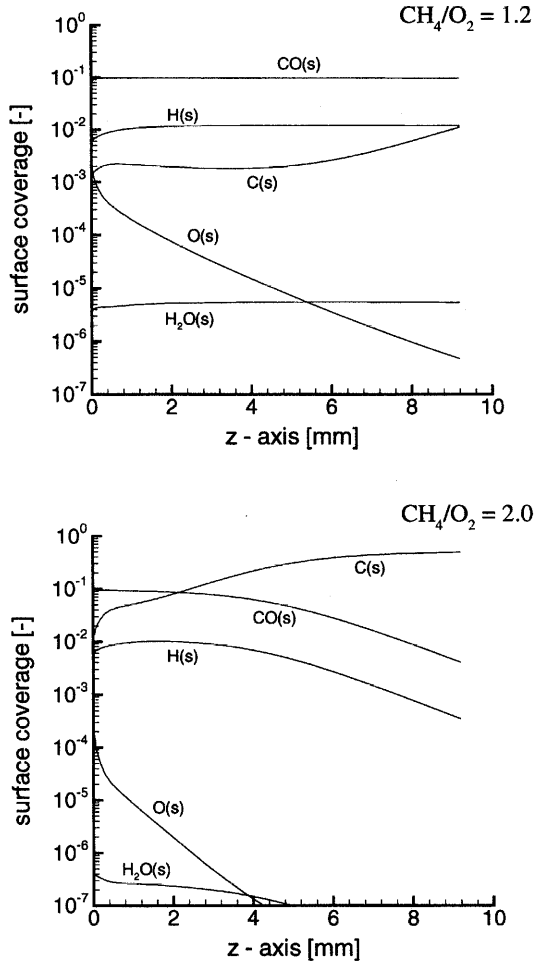

Figure 11. Surface coverage as a function of the axial position (z) for a CH_4/O_2 ratio of 1.2 (top) and 2.0 (bottom).

Rh catalyst, $d = 0.25$ mm, 30% N_2 as diluent, $p = 1.4$ bar, $T_{cat} = 1273$ K, $u_{in} = 1$ m/s. The axial position is zero at the catalyst entrance. The simulation does not include gas-phase chemistry.

Role of gas-phase chemistry at high pressure

The industrial application of short-contact-time reactors depends on the possibility of running the reaction at higher pressures. In laboratory experiments, measurements of the pressure dependence are limited due to safety and costs. The likelihood that gas-phase reactions will affect syngas selectivity and methane conversion becomes higher at elevated pressure. A former study, in which gas-phase reactions were neglected, demonstrated the decrease of methane conversion with increasing pressure while the syngas selectivity decreases only slightly at higher pressure (Deutschmann and Schmidt, 1998). Now, we extend this study, also using a gas-phase reaction model.

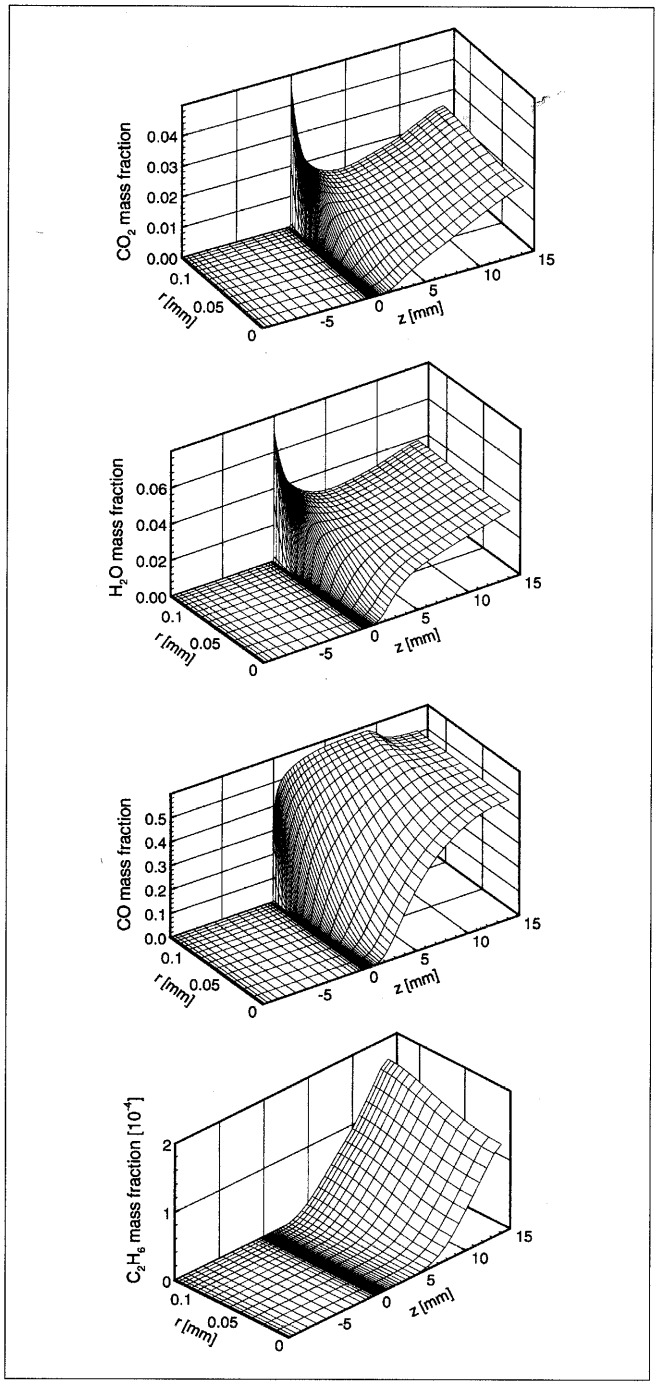

Figure 12. Gas-phase species profiles at elevated pressure of $p = 10$ bar.

Rh catalyst, $d = 0.25$ mm, CH_4/O_2 ratio of 2.0 (20% N_2 as diluent), $T_{cat} = 1188$ K, $u_{in} = 3.7$ m/s. The axial position (z) is zero at the catalyst entrance and the catalytic wall is at the radial position (r) of 0.125 mm. The simulation includes gas-phase chemistry.

The following reactor conditions are used in the simulation: methane/oxygen ratio of 2 with 20% (volume) nitrogen as diluent, gas inlet velocity of 3.7 m/s, pore diameter 0.25 mm, catalyst temperature of 1,188 K, and pressure of 10 bar. Figure 12 exhibits gas-phase profiles of CO_2, H_2O, and CO mass fraction, all of which can be produced on the surface as well as in the gas phase. Furthermore, the ethane profile is shown, a species that is exclusively formed in the gas phase.

The reactor is not long enough for complete conversion of methane, so the conversion of methane is 79% and that of oxygen is 90%. A radial gradient of CO is also still present near the exit of the catalytic part of the reactor ($z = 10$ mm). In the catalyst entrance region, the complete oxidation takes place on the surface as already shown in the baseline case being at atmospheric pressure. However, the formation of CO_2 and H_2O continues behind this entrance region, mainly because of gas-phase reactions. The influence of the gas-phase chemistry can clearly be seen from the fact that the CO_2 and H_2O formation continues behind the catalytic section of the reactor ($z > 10$ mm). A small but significant ethane production starts in the middle of the catalytic reactor ($z \sim 5$ mm) indicating a delay time before gas-phase reactions become significant. The mass fraction of ethane has increased by six orders of magnitude in comparison to the atmospheric pressure simulation (Figure 3).

In summary, gas-phase reactions lead to an increase of undesired complete oxidation products and formation of methane coupling products at a pressure of 10 bar. A comparison between the full (surface plus gas-phase reactions) simulation and the simulation that neglects gas-phase reactions reveals only a few percent variation in the product composition: the conversion of methane is almost constant (79%) while the oxygen conversion increases from 86% to 90%. The selectivities of CO_2 and H_2O increase from 1.2% to 3% and from 3.8% to 5.5%, respectively. However, homogeneous reactions are expected to become more and more significant at even higher pressures of 20–30 bar at which an industrial application should be operated.

Conclusions

A 2-D elliptic model based on the CFD code FLUENT has been coupled with external subroutines to describe detailed surface and gas-phase chemistry in short-contact-time reactors. We have applied these numerical tools to simulate the partial oxidation of methane in rhodium- and platinum-coated monoliths using elementary step reaction mechanisms and detailed transport models. The simulation describes the complex interaction between mass transfer and heat transfer as well as chemistry. At the catalyst entrance, an extremely rapid variation of temperature, velocity, and transport coefficients occurs. The complete oxidation products, CO_2 and H_2O, are catalytically formed in the entrance region of the reactor. The

different behavior of rhodium and platinum catalysts in syngas formation is explained by the surface reaction steps. Methane conversion and syngas selectivity decrease with increasing flow velocity. A larger pore diameter reduces conversion. Increasing methane/oxygen ratio leads to higher selectivity, although it is compensated for by decreasing methane conversion for a ratio over 2. Gas-phase reactions can be neglected if the reactor is run at atmospheric pressure. However, at pressures over 10 bar gas-phase reactions lead to significant variation of selectivity and conversion. Here, complete oxidation (combustion) of methane rises and coupling products such as ethane are formed.

The straight tube geometry is a simplified model of a pore in a catalytic monolith with its tortuous pathways. We are currently working on model development to take this tortuosity into account. In the cases studied here, no temperature gradient was experimentally observed along the axial direction of the catalytic wall, and a constant catalytic wall temperature was assumed in the simulation. However, a model of an energy balance in the solid will be used to simulate chemical systems where large temperature variations along the catalyst occur (Hohn et al., 1998). Radical adsorption and desorption are neglected in these calculations because these steps have so far not been incorporated into surface reaction mechanisms for partial oxidation of methane. An improved reaction scheme is under development and will be used in future studies. This will be especially important in describing reactor performance at high pressures.

Acknowledgments

The authors would like to thank Professor J. Warnatz for his continuous support in modeling catalytic combustion systems. This research is supported by using the computer facilities of the Supercomputer Institute at the University of Minnesota. Financial support by DOE under Grant No. DE-FG02-88ER13878-A02 is acknowledged. O.D. gratefully acknowledges a grant from the DFG (Deutsche Forschungsgemeinschaft) for a one-year stay at the University of Minnesota Department of Chemical Engineering and Materials Science.

Literature Cited

Bodke, A. S., and L. D. Schmidt, "The Effect of Ceramic Supports on Partial Oxidation of Hydrocarbons over Noble Metal Coated Monoliths," *J. Catal.*, **179**, 138 (1998).

Deuflhard, P., E. Hairer, and J. Zugk, "One-Step and Extrapolation Methods for Differential-Algebraic Systems," *Num. Math.*, **51**, 501 (1987).

Deutschmann, O., R. Schmidt, F. Behrendt, and J. Warnatz, "Numerical Modeling of Catalytic Ignition," *Int. Symp. on Comb.*, p. 1747, Combust. Inst. (1996).

Deutschmann, O., F. Behrendt, and J. Warnatz, "Formal Treatment of Catalytic Conversion and Combustion of Methane," *Catal. Today*, in press (1998a).

Deutschmann, O., and L. D. Schmidt, "Two-Dimensional Modeling of Partial Oxidation of Methane on Rhodium in a Short Contact Time Reactor," *Int. Symp. on Comb.*, Combustion Inst. (1998b).

Goetsch, D. A., and L. D. Schmidt, "Microsecond Catalytic Partial Oxidation of Alkanes," *Science*, **271**, 1560 (1996).

Hickman, D. A., and L. D. Schmidt, "Steps in CH_4 Oxidation on Pt and Rh Surfaces: High-Temperature Reactor Simulations," *AIChE J.*, **39**, 1164 (1993).

Hohn, K. L., P. M. Witt, M. B. Davis, and L. D. Schmidt, "Methane Coupling to Acetylene over Pt Coated Monoliths at Millisecond Contact Times," *Catal. Lett.*, **54**, 105 (1998).

Raja, L. L., R. J. Kee, and L. R. Petzold, "Simulation of the Transient, Compressible, Gas-Dynamic, Behavior of Catalytic-Combustion Ignition in Stagnation Flows," *Int. Symp. on Comb.*, Combustion Inst. (1998).

Schmidt, L. D., O. Deutschmann, and C. T. Goralski, Jr., "Modeling the Partial Oxidation of Methane to Syngas at Millisecond Contact Times," *Gas Conv. Symp.*, Taormina, Italy (Sept. 20–25, 1998).

Veser, G., J. Frauhammer, and L. D. Schmidt, "Catalytic Ignition of Methane Oxidation in a Monolithic Reactor," AIChE Meeting, Paper 266d, Los Angeles (Nov. 16–21, 1997).

Warnatz, J., M. D. Allendorf, R. J. Kee, and M. E. Coltrin, "A Model of Elementary Chemistry and Fluid Mechanics in the Combustion of Hydrogen on Platinum Surfaces," *Combust. Flame*, **96**, 393 (1994).

Warnatz, J., "Hydrocarbon Oxidation Reaction Mechanism," personal communication (1998).

Witt, P. M., and L. D. Schmidt, "Effect of Flow Rate on the Partial Oxidation of Methane and Ethane," *J. of Catal.*, **163**, 465 (1996).

Manuscript received June 11, 1998, and revision received Sept. 14, 1998.